Thin Solid Films 556 (2014) 552–559

Contents lists available at ScienceDirect

Thin Solid Films

journal homepage: www.elsevier.com/locate/tsf

Growth and opto-electro-structural properties of nanocrystalline PbSe thin films

H.M. Ali [a,b], S.A. Saleh [a,c]

[a] Physics Department, Faculty of Science, Sohag University, P.O. 82524, Sohag, Egypt
[b] Physics Department, Faculty of Science, Al-Baha University, P.O. 1034, Al-Baha, Saudi Arabia
[c] Physics Department, College of Science & Arts, Najran University, P.O. 1988, Najran, Saudi Arabia

A R T I C L E I N F O

Article history:
Received 29 May 2013
Received in revised form 5 January 2014
Accepted 23 January 2014
Available online 31 January 2014

Keywords:
Thin films
Lead selenide
Vapor deposition
Optical properties
Electrical conductivity

A B S T R A C T

The present work deals with the structural, optical and electrical characterization of PbSe thin films with variable thickness deposited on well-cleaned glass substrates by electron beam evaporation technique at room temperature (RT). Grown films are characterized by X-ray diffraction, energy dispersive spectroscopy, resistivity measurements (from room temperature to 200 °C) and optical measurements at room temperature in order to study their various properties. The optical constants (namely, absorption coefficient, the refractive index, extinction coefficient, real and imaginary part of dielectric constant) have been studied for as-deposited PbSe thin films as a function of photon energy in the wavelength range 400–2500 nm at RT. The thickness dependence of optical constants was discussed.

© 2014 Elsevier B.V. All rights reserved.

1. Introduction

In recent years, thin semiconductor films have been deemed technologically important in the fabrication of large area photodiode arrays, solar selective coatings, solar cells, photoconductor, sensors, etc. [1]. Lead salt thin films have a number of applications in various devices such as thermoelectric devices, infrared detectors, photoresistors, lasers, solar cells, chemical sensor and other electronic devices [2–7]. As a member of the $A^{IV}B^{VI}$ lead salt semiconductor family, lead selenide (PbSe) is semiconducting with good grade of polarity, with bonds formed through electrostatic interactions among the ions of the crystal lattice, crystallizing in the rock-salt type structure [8]. Moreover, PbSe has many special semiconductive properties such as a narrow band gap, high dielectric constant, high carrier mobility, high transmittance rate and positive temperature coefficient [8,9] and has extensive commercial applications such as infrared (IR) detectors, lasers and thermoelectric energy converters [10]. To achieve applicable PbSe film based optoelectronic devices, considerable experimental investigations have been focused on the preparation of high quality optical thin films with stable physical (opto-electro-structural) properties.

Owing to their unique optical, electrical and semiconducting properties, PbSe thin films form the mainstay of the electronic industry and the cornerstone of modern technology. In this class of materials, the change in its band gap is thought to be due to sharp cut-off of the wavelength with spectral transmittance instead of slow increase [11], wide range of stoichiometric deviation, the presence of large number of dislocations, changes in barrier height because of variation in grain size in polycrystalline films and quantum size effect [12]. The quantum efficiency is high due to the direct band gap [13]. The combination of momentum conversation with fast response which has made the direct band gap film is always preferred over indirect one [1]. This is the main motivation to study PbSe thin films.

A number of deposition techniques have been used to grow the thin films such as thermal evaporation [14], electron beam evaporation [15], sputtering evaporation [16], flash evaporation [17], molecular beam epitaxy [18], pulsed laser ablation [19], chemical vapor deposition [20] and chemical bath deposition [21]. All these techniques have some advantages and some limitations, largely discussed in literature (see [22]). Particularly, the thermal evaporation technique caused much attention due to its relative simplicity, ease of process control and scalability to large areas and high throughout [23]. The main drawback associated with the thermal evaporation of source material is the poor transfer of stoichiometry from a multi-component starting alloy to the deposited film. In addition, phase separation in the melt can result in splashing of molten material from the boat that can contaminate the film [24]. This disadvantage can be avoided by the electron beam evaporation.

PbSe has been deposited on different substrates such as Silicon (Si) substrate [19] and metal substrate [25]. For PbSe deposited on Si substrate, it was found that the layers have large mechanical strains due to that the silicon substrate has a much smaller thermal expansion coefficient than PbSe. For PbSe deposited on metal substrate it was found that the potential applied and the composition of the

E-mail addresses: hazem95@yahoo.com (H.M. Ali), saleh2010_ahmed@yahoo.com (S.A. Saleh).

0040-6090/$ – see front matter © 2014 Elsevier B.V. All rights reserved.
http://dx.doi.org/10.1016/j.tsf.2014.01.057

electrolyte were found to be the critical factors determining the substructure and composition of a product.

The structure of the thin films strongly influences the electronic properties and is highly dependent upon the preparation technique and deposition conditions [26]. The optical, electrical, mechanical and structural properties of thin films can be tailored by controlling the composition and deposition parameters such as the deposition time, namely thickness. The thickness plays an important role in the properties of the film. However, the thickness dependence of the physical properties of bismuth and zinc chalcogenides has been recently receiving special attention [27–30]. In this work, we have reported the effects of the film thickness on the opto-electro-structural properties of the nanocrystalline PbSe films deposited on well-cleaned glass substrates by electron beam evaporation technique.

2. Experimental details

In the present investigation the bulk alloy of PbSe was prepared by melt-quenching technique. High purity (5N) of materials were weighted using a microbalance according to their atomic percentages and were sealed in quartz ampoule with a vacuum ~10^{-5} Torr. The ampoule containing the materials was heated to 850 °C and held at this temperature for 10 h. During the melt process, the ampoule was rocked frequently to make the melt homogenous. After that, the obtained melt was cooled rapidly by removing the ampoule from the furnace and dropping it to ice-cooled water.

PbSe alloy was deposited using electron beam evaporation technique in Edward's high vacuum coating unit model E306A to obtain lead selenide films. The deposition conditions were: (1) a vacuum of 2.66×10^{-3} Pa, (2) an accelerating voltage of 4 kV, (3) and electron beam current 10–12 mA.

The PbSe films of various thicknesses were deposited on ultrasonically cleaned glass substrates kept at 300 K. The films of different thicknesses (100, 150, 175, 200, and 250 nm) were deposited under almost same environment. The film thickness was measured by a digital thickness monitor (TM200 Maxtek). The elemental compositions of the specimens were checked using energy dispersive spectroscopy (EDS) and the estimated average precision was about 1% in atomic fraction for each element. Structural property of the as-deposited films with thickness in between 100 and 250 nm was studied by X-ray diffractometer, type PANalytical (X' pert Pro MPR) in the scanning angles 10–70° (2θ). The wavelength used was 0.15406 nm.

A Jasco V-570 UV–VIS–NIR spectrophotometer was employed to record the transmission and reflection spectra over the wavelength range 200–2500 nm at both normal incidence and room temperature. Diffuse reflectance spectra were obtained using a diffuse reflectance accessory model ISN-470, and the reflectance was converted by the instrument software to F(R) values according to the Kubelka–Munk method. The electrical resistivity of the films was measure by d.c. two-point probe method in the temperature range 300–490 K as previously reported [31].

3. Results and discussion

3.1. EDS and XRD analyses

The EDS spectrum shown in Fig. 1 of the PbSe films display that the as-deposited film is free from any other impurities and provides the mass fraction of each element, i.e. lead and selenium, used during the deposition process as well as measured via EDS. The elemental analysis of the films was carried out to study the stoichiometry of the specimens. All films are nearly stoichiometric with the Pb:Se ratio of ~1 confirmed by the EDS analysis. However, the atomic percents for each element at different spots of all films were averaged and compared to the nominal atomic percent of the corresponding compound. The chemical composition measured by EDS also showed no observable difference among the films.

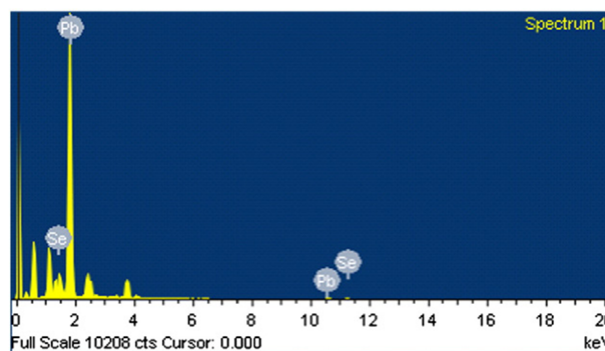

Fig. 1. The EDS spectrum of the PbSe thin film.

XRD analysis was performed to investigate the effects of the film thickness on the crystallinity and crystal phase of the films. The XRD patterns of PbSe films with various thicknesses (in the range 100–250 nm) are shown in Fig. 2. From these X-ray patterns, one can clearly observe that all the films have a strong (002) peak. Strong preferential growth is observed along (002) plane, suggesting that the cubic (rock-salt Fm−3 m (NaCl)) structure films to be single-phase and well-oriented with a (002) texture. Moreover, the as-deposited PbSe films showed cubic phase with a preferential c-axis orientation along the (002) plane. The formation mechanism of the preferential oriented thin films may be related to the minimization of surface energy [32]. For the thinnest film, the broad peak of XRD patterns shows nanocrystalline in nature of PbSe thin films. The peak becomes sharp and some peaks appeared at high '2θ' values with increasing film thickness. The plane indices are obtained by comparing the intensities and positions of the peaks with those of PbSe which are given by (ICSD PDF: 006-0354).

By fitting the XRD peaks, the peak position, relative peak intensity, inter planer distance, lattice parameters, the crystallite size, the dislocation density, the strain and the number of crystallites per unit area are obtained and given in Table 1. The peak intensities have been normalized.

The inter planer distance (d_{hkl}) is experimentally determined from Bragg's relation as follows:

$$2d_{hkl}\sin\theta = n\lambda \tag{1}$$

where θ is the corresponding Bragg's angle, n is a factor equal to unity, and λ is the wavelength of X-ray used.

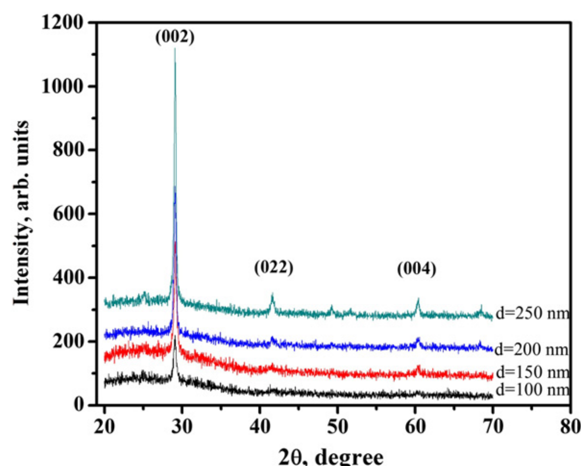

Fig. 2. X-ray diffraction pattern of PbSe thin films with different film thicknesses.

Table 1
XRD-parameters of the as-deposited films.

Thickness (nm)	2θ	Int.	FWHM	$d_{(002)}$-spacing	C_s (nm)	ε (10^{-4})	ρ $(nm)^{-2}$ (10^{-3})	N (10^{14})/cm^2
100	29.089	130	0.384	3.06627	17.2	19.9	3.38	1.97
150	29.093	339	0.2165	3.06707	25.1	13.7	1.59	0.95
200	29.099	438	0.1968	3.06735	35.4	9.68	0.97	0.45
250	29.113	725	0.1378	3.06755	39.7	8.63	0.86	0.40

The lattice parameter (a) of cubic system is estimated from the following equation [33],

$$a = d_{hkl}\left(h^2 + k^2 + l^2\right)^{0.5}. \quad (2)$$

The crystallite size (C_s) has been deduced from the full width at half maximum (*FWHM*) of the most intense peak of the respective crystals using Sherrer's formula [34],

$$C_s = \frac{0.9\lambda}{\beta \cos\theta} \quad (3)$$

where both λ and θ are as mentioned above, and β (the *FWHM* of the peak) is expressed in radians and corrected for the instrumental broadening by measuring the width of a standard reference.

The dislocation density (ρ), which represents the amount of defects in the crystal, is calculated from the following equation [35]:

$$\rho = \frac{1}{C_s^2}. \quad (4)$$

The strain is one of the binary predominant factors which broaden the diffraction peaks. The very small crystalline size in nanoscale is expected to result in lattice strain [36]. It was calculated as follows:

$$\varepsilon = \beta \cos\theta / 4. \quad (5)$$

The number of crystallites per unit area (N) of the nanocrystallites has been obtained using the relationship [37],

$$N = \frac{t}{C_s^3} \quad (6)$$

where t is the film thickness.

From the normalized peak intensities, it can be seen that all the films have a strong diffraction peak along [002] direction. As the film thickness increased, the peaks became sharper and some peaks appeared at high 2θ values suggesting improved crystallinity. However, a minor shift is observed in the peak positions indicating a small change in the lattice parameter. Considering the variations in the crystallite size and the peak intensities with the thickness of the film, it can be suggested that the crystallinity of PbSe films has been improved. It is observed that crystallite size increases with thickness. Due to that, the defects in the lattice are decreased, which in turn reduces the stress, internal microstrain and dislocation density [28,38]. The small values of ρ obtained in the present work confirm the good crystallinity of the films [37]. The increase in peak intensity and decrease of (*FWHM*) are due to the improvement in the crystallinity and a reduction in the microstrain. From these results, the film crystallinity is enhanced when the thickness is increased.

3.2. Optical measurements

Fig. 3-a illustrates the optical transmittance of nanocrystallite PbSe films in the wavelength range from 200 to 2500 nm for various film thickness. It can be observed that the optical transmittance spectra of the films show a strong dependence on the film thickness and a fall of transmittance (sharp edge) at the band edge which is an indication of good crystallinity of the deposited films. Above the absorption edge, it is well known that the low transmittance of the deposited films mainly results from the high film thickness. Moreover, the transmission spectra of the films show that the film thickness shifts optical

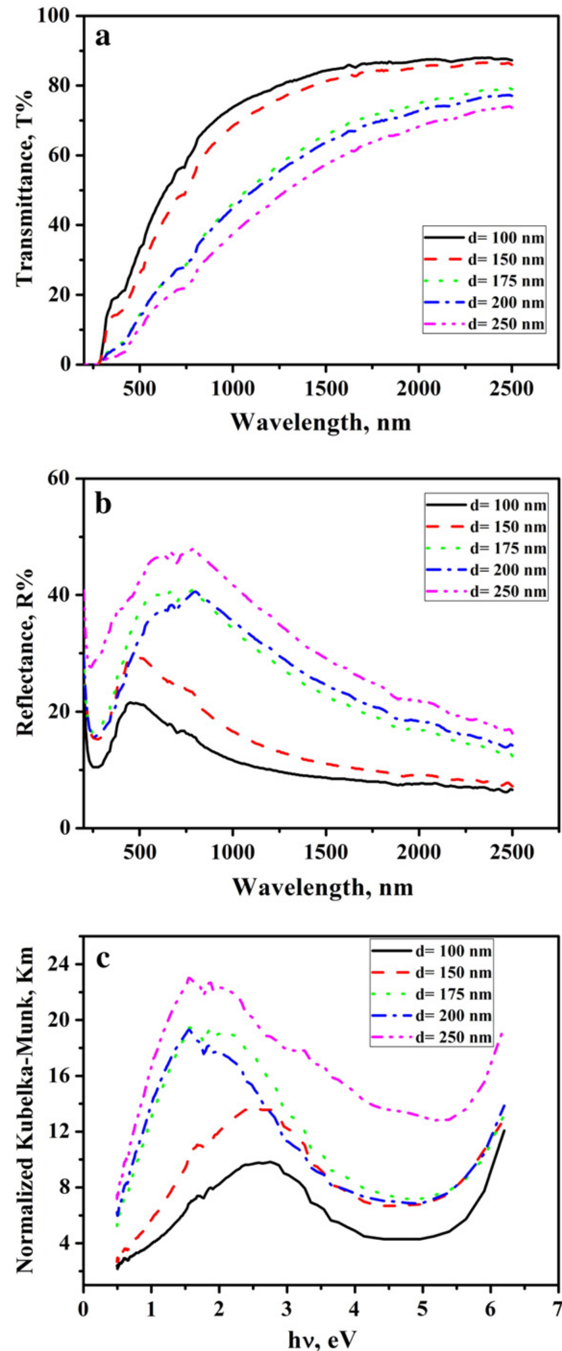

Fig. 3. The optical transmittance, (a), reflection (b) and normalized Kubelka–Munk function of PbSe thin films with different thicknesses.

transmission edge to higher wavelength. Since the transmission through the thin film decreases by the increase of the thickness, it is clear that there is no possibility of formation of cracks and pinholes in the films [39]. In other words, two different effects are observed in the transmittance spectra of the films: (I) the average transmittance of PbSe film decreases with increasing the film thickness in the visible range and (II) the optical transmission edge has been shifted to longer wavelengths. Thus, the film thickness is a key parameter in the preparation of film for various applications [40]. The presence of a single slope in the curves suggests that films prepared by using electron beam evaporation are single phase in nature and the type of transition is direct and allowed; these observations are in concurrence with the earlier studies as several researchers reported this type of transition [41]. Hence, the onset of the transmittance is located at the optical band gap which is due to the fact that the PbSe is a direct–allowed band gap semiconductor.

The PbSe films were analyzed also by optical reflectance as shown in Fig. 3-b. The diffuse reflection spectra were measured at room temperature and converted to absorption spectra using the Kubelka–Munk theory [42,43] as follows:

$$\mathrm{F(R)} = (1-\mathrm{R})^2/2\mathrm{R} \tag{7}$$

where R is the diffuse-reflection factor as shown in Fig. 3-c. One can see that the PbSe films exhibit one band. Such a shift in the bands to lower energy values, suggests a decrease in the optical energy gap with increasing the film thickness.

The direct–allowed band gap of the deposited films has been deduced by three procedures. The first one was obtained by extrapolation of the linear relationship between $(\alpha h\nu)^2$ and $(h\nu)$ according to the following equation [44–46] as shown in Fig. 4-a:

$$(\alpha h\nu)^2 = \beta\left(h\nu - E_{g(1)}^{opt}\right) \tag{8}$$

where $h\nu$ is the incident photon energy, the edge width parameter β represents the film quality, and $E_{g(1)}^{Opt}$ is the direct–allowed band gap of a material.

The second procedure for the determination of $(E_{g(2)}^{Opt})$ was estimated using the optical absorption coefficient evaluated from Kubelka–Munk function (Eq. (7)), the optical gaps of the films were determined by extrapolating the linear portion of the plots of $[\mathrm{F(R)}h\nu]^2$ versus $h\nu$ as seen in Fig. 4-b.

The third method for obtaining the optical energy gap was calculated by plotting $h^2\nu^2\varepsilon_2$ against $h\nu$ near the absorption edge as shown in Fig. 4-c using the following equation [47]:

$$h^2\nu^2\varepsilon_2 \approx \left(h\nu - E_{g(3)}^{Opt.}\right) \tag{9}$$

where ε_2 is the imaginary part of the dielectric constant.

The corresponding optical energy gap, calculated using the above three methods is shown in Fig. 4-d. The figure states that, the magnitudes of the optical energy gaps, which were obtained using the different methods, are approximately the same and the deviations are in the range of error bars. Upon increasing the film thickness from 150 to 250 nm, the optical energy gap decreased from 1.24 to 0.7 eV. The lower value of the optical band gap at higher film thickness is due to the large grain size developed at higher thickness

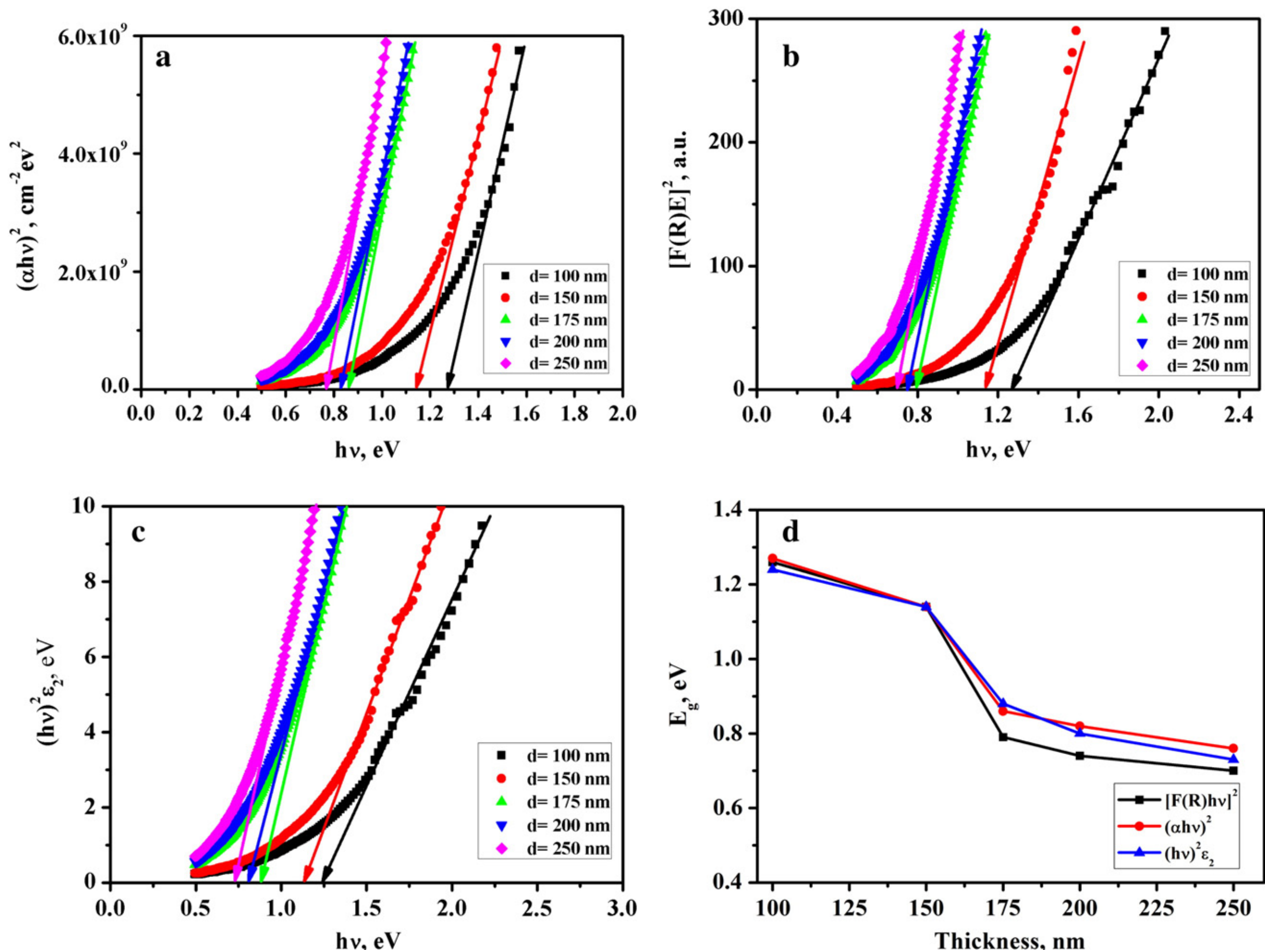

Fig. 4. Plots of $(\alpha h\nu)^2$, $[\mathrm{F(R)\ E}]^2$, $[(h\nu)^2\ \varepsilon_2]$ versus hν and the corresponding $\mathrm{E_g}$ of PbSe films with different thicknesses.

and a low density of the defects [28]. This might be explained as being because the samples would have more perfect crystallization and a low density of the defects. These defects are responsible for the presence of localized states in the band gap [48]. In addition the red-shift of optical band gap in the present specimens was due to the influence of the size effect on the energy level of confined excitons, because the average size of the nanoparticles obviously became bigger with an increase of the film thickness [49]. It is observed that the cut-off wavelength shifts towards red with the increase of film thickness (see Fig. 5).

Another important parameter for characterizing the electronic properties of semi-conducting materials is the Urbach energy (E_u) which is interpreted as the width of tails of localized states in the gap region. The Urbach energy, E_u values were calculated from the inverse of the slope of the straight line of the relation ln α vs. $h\nu$. The corresponding values of the Urbach energy are shown in Fig. 6. It is observed that the Urbach energy increases as the film thickness increases. The increase in Urbach energy and red-shift of optical band gap with increasing the film thickness indicates that the width of localized states increased thereby reducing the optical energy gap.

Knowledge of the dispersion of the refractive indices of semiconductor materials is necessary for accurate modeling and design of devices [40]. Moreover, refractive index is necessary for the design and modeling of optical components and optical coating such as interference filters. The theory of reflectance of light from a thin film is expressed in terms of Fresnel's coefficient. The values of refractive index (n), and extinction coefficient (k) for the examined films were computed from the obtained R(λ) using the following relations [50],

$$k = \frac{\alpha\lambda}{4\pi} \tag{10}$$

$$n = \frac{1+R}{1-R} \pm \left[\left(\frac{R+1}{R-1}\right)^2 - \left(1+k^2\right)\right]^{\frac{1}{2}} \tag{11}$$

where R is the reflectivity. The dependence of both k and n values of the films on wavelength is shown in Fig. 7-(a,b). It is evident that, both n and k values increase with increasing film thickness. So, the film thickness has an important effect on the refractive index, and extinction coefficient. The increase in refractive index with increasing the film thickness can be attributed to the increase of the film density and/or the improvement of the films crystallinity [51].

The film packing density was estimated from the following expression [52]:

$$n_f^2 = \frac{(1-p)\ n_v^4 + (1+p)\ n_v n_s^2}{(1+p)\ n_v^2 + (1-p)\ n_s^2} \tag{12}$$

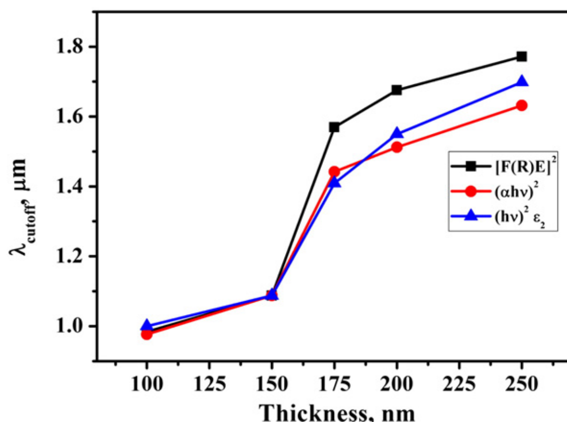

Fig. 5. The thickness dependence of cutoff wavelength.

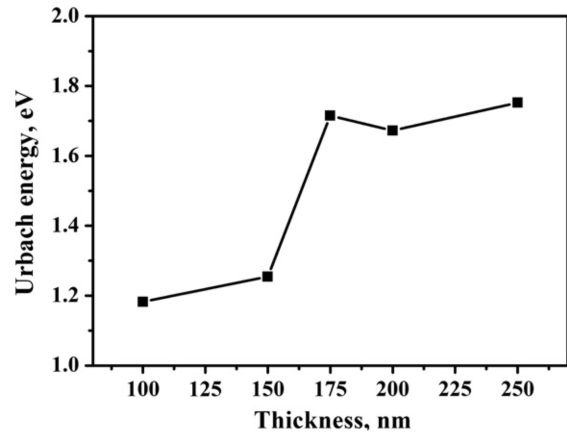

Fig. 6. Plot of Urbach energy as a function of film thickness.

where n_f is the refractive index of composite film, n_s is the index of the solid material of the film, n_v is the index of the void in the film (equals one for air), and P is the packing density. The behavior of the backing densities with respect to the film thickness is shown in Fig. 7-c. It is evident that the calculated packing density values increase with increasing the thickness of the film.

The dispersion plays an important role in the research for optical materials, because it is a significant factor in optical communication and in designing devices for spectral dispersion. The high frequency properties of PbSe thin films can be treated as a single oscillator. The spectral dependence of the refractive index (n), in the visible and near infrared regions, has been analyzed in terms of the well-known Wemple–DiDomenico single effective oscillator model [53]. According to this model, the relation between the refractive index and the single oscillator strength below the band gap is given by the expression:

$$\frac{1}{n^2-1} = \frac{E_o}{E_d} - \frac{(h\nu)^2}{E_o E_d} \tag{13}$$

where E_o and E_d are single oscillator constants, which are represented by the energy of the effective dispersion oscillator and the dispersion energy, respectively, which measures the average strength of interband optical transitions. The values of E_o and E_d can be evaluated from the plot of $(n-1)^{-1}$ versus $(h\nu)^2$ as presented in Fig. 8-a. The estimated values of the parameters E_o and E_d for different thicknesses of PbSe film are depicted in Fig. 8-b.

The fundamental electron excitation spectrum of the films was described by means of the frequency dependence of the complex electronic dielectric constant. The complex dielectric function can be defined as [40]:

$$\varepsilon^* = \left(n^2 - k^2\right) + i2nk \tag{14}$$

where the first term of this equation is the real part of the dielectric constant (ε_1) and the second term is the imaginary parts of dielectric constant (ε_2). The real and imaginary parts of the dielectric constant are expressed by [54]:

$$\varepsilon_1 = n^2 - k^2 = \varepsilon_i - \left(\frac{e^2 N}{4\pi c^2 \varepsilon_o m^*}\right)\lambda^2 \tag{15}$$

$$\varepsilon_2 = 2nk \tag{16}$$

where (n) is the refractive index, (k) is the extinction coefficient, ε_∞ is the optical dielectric constant, e is the charge of the electron, N is the free charge-carrier concentration, ε_o is the vacuum permittivity, m^* is the effective mass of the electron and c is the speed of light.

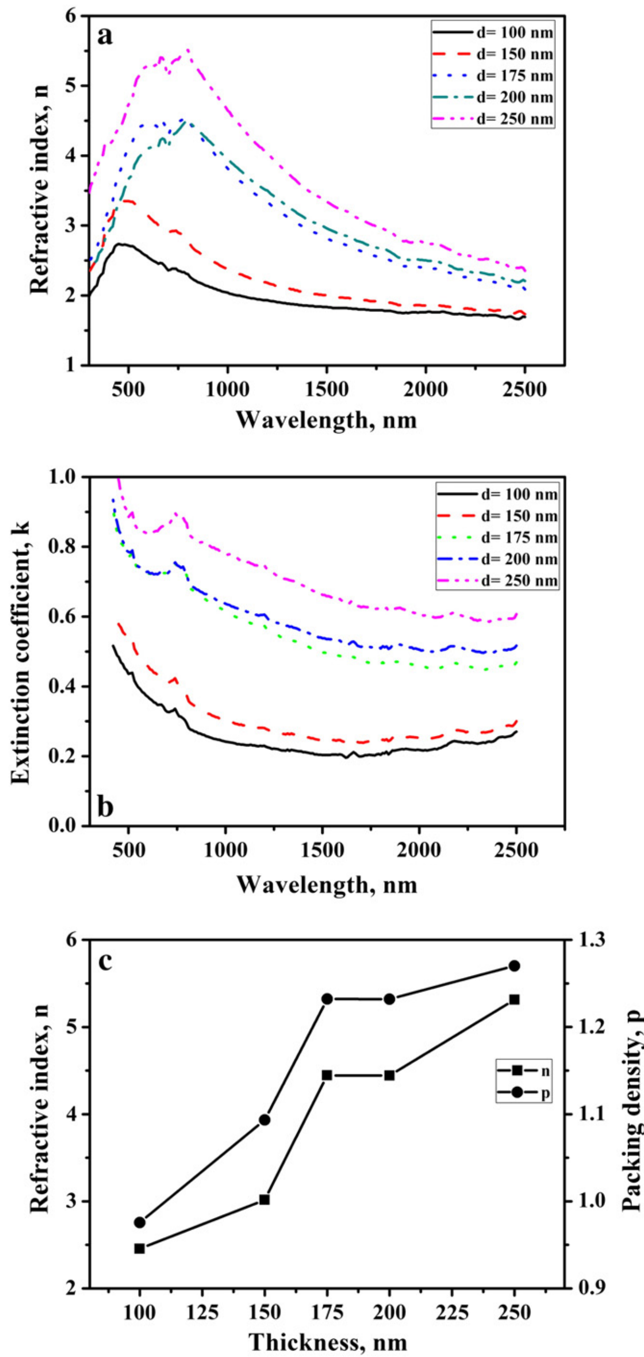

Fig. 7. Variations of the refractive index (a) and extinction coefficient (b) with wavelength; and the thickness dependence of refractive index in the visible region and packing density of PbSe films (c).

Values of optical dielectric constant, ε_i, can be estimated from the extrapolation of the straight-line potion of the ε_1 versus λ^2 plot at longer wavelengths (in the transparent region $k = 0$) for different thicknesses of PbSe films as shown in Fig. 9-a,b. The ratio of N/m* can be determined for the as-deposited films from the slopes of these lines. The calculated free carrier concentration and effective mass are shown in Fig. 9-c. Based on Fig. 9-b&c, one can see that the values of ε_i and N increase with increasing the film thickness. The increase in the concentration of free carriers will enhance the conductivity [55]. The change of these parameters with film thickness indicates that the film thickness has an important effect on them.

The dielectric tangent or loss factor (tan δ) which is represented as dissipated energy in a dielectric system, is proportional to the loss of energy from the applied field into the sample. The loss factor of PbSe thin films can be calculated with the help of the real (ε_1) and imaginary (ε_2) parts of the dielectric constant according the following equation:

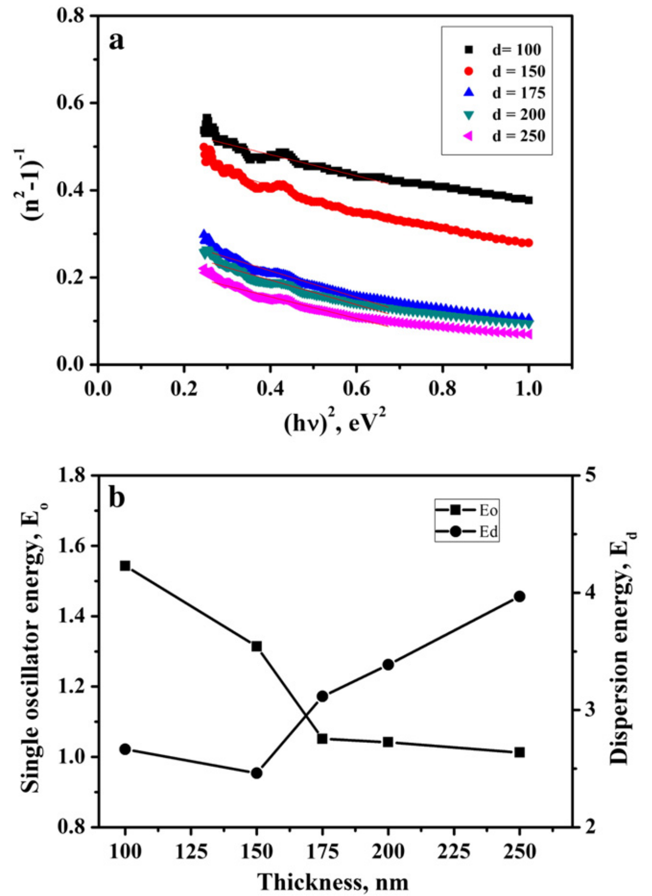

Fig. 8. Plots of $(n^2-1)^{-1}$ versus $(h\nu)^2$ for PbSe film with different thicknesses (a) and the variations of E_o and E_d with film thickness (b).

$$\tan\delta = \frac{\varepsilon_2}{\varepsilon_1}. \quad (17)$$

The variation of tan δ for different films thickness of PbSe as a function of frequency is shown in Fig. 10. It is clear that the dielectric tangent increases with increasing frequency. Moreover, the general trend can be depicted that tan δ is found to increase with increasing frequency. The observed behavior may be due to different mechanisms of polarization [56].

3.3. Electrical measurements

The electrical conductivity measurement was carried out in the temperature range 300–460 K for all the films under dark. Fig. 11 shows the dependence of the two-probe dc conductivity (σ_{dc}) versus reciprocal temperature, measured in the range of 30–200 °C at a fixed rate of 10 °C/min, for films with different thicknesses. The conductivity of all films increases with the increase in temperature showing the semiconducting behavior of the films [33]. According to the experimental results, the dc conductivity of various films can be expressed by an Arrhenius type relation:

$$\sigma_{dc} = \sigma_o \ \exp\left(\frac{-E_\sigma}{K_B T}\right) \quad (18)$$

where the pre-exponential factor σ_o depends on the film composition [57], E_σ is the conduction activation energy, and K_B is Boltzmann

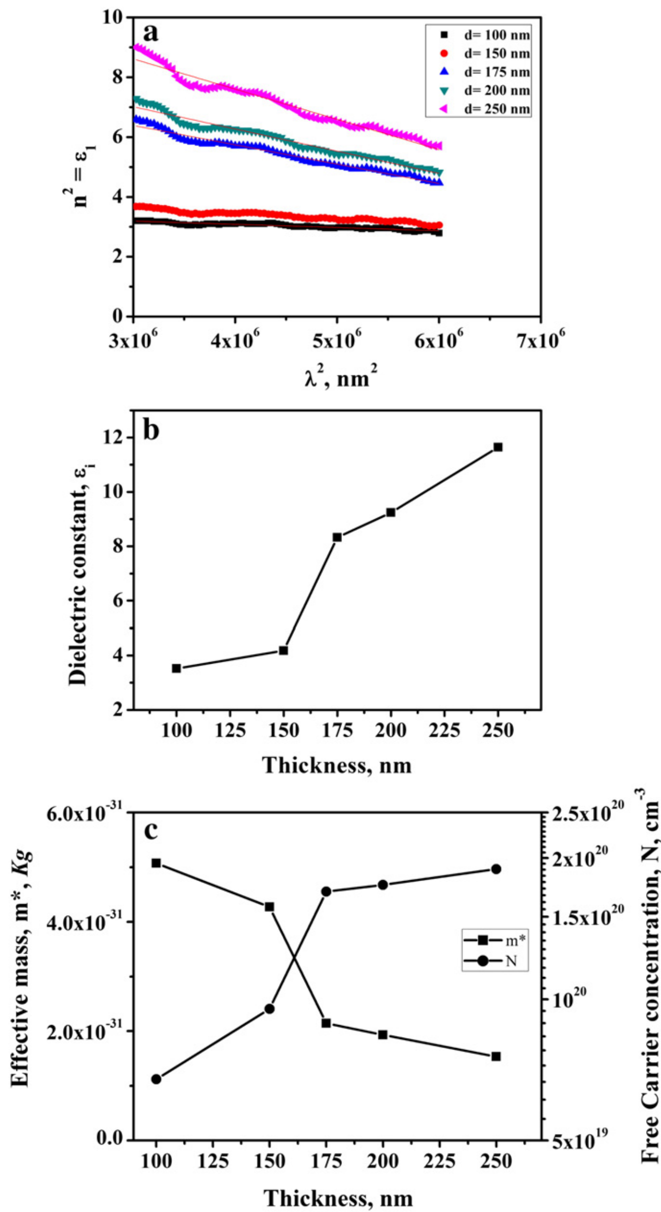

Fig. 9. Plots of the real dielectric constant ε_1 versus the square of wavelength (a); the thickness dependence of the residual dielectric constant ε_i (b); variations of effective mass and free carrier concentration with film thickness (c).

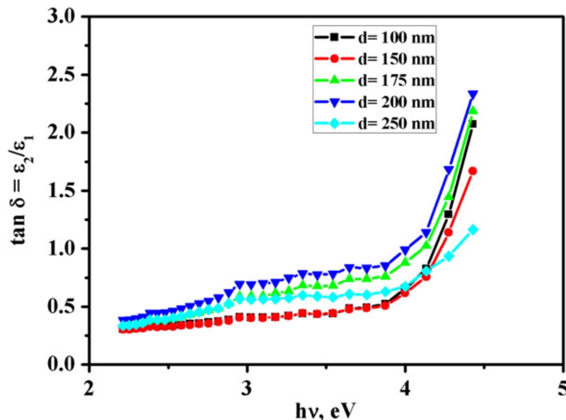

Fig. 10. Plots of tan δ for different films thickness of PbSe as a function of frequency.

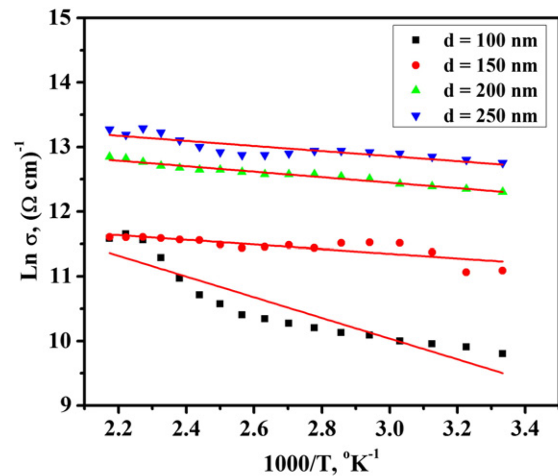

Fig. 11. Ln σ versus 1000/T plot as a function of film thickness.

constant. The linear dependence of ln σ with 1/T indicates a thermally activated conduction mechanism for the conductivity in the considered range of temperature. Similar results have been reported previously [4,6]. The activation energy for conduction is the energy required to take place between the defect level and valence or conduction band. The two-probe method of conductivity measurement shows that the as-deposited films have resistivity of the order of 10^6 Ω cm at room temperature. The high resistivity of the film may be due to high grain boundary density, discontinuities and small grain of the film. Based on Fig. 11, it is clear that σ increases with increasing film thickness. Such behavior can be attributed to lattice defects such as vacancies, interstitials and dislocations, which developed through the first stage of the film growth during deposition. These defects add an extra one percent to the resistivity. As the film thickness increases, these defects diffuse and, accordingly, the corresponding resistivity decreases and hence the conductivity increases with thickness. The increase of the conductivity was due to the increase in the carrier concentration and the better crystallinity of PbSe thin films and its dense microstructure with relative larger grain sizes as seen from XRD. An additional explanation for enhanced conduction is related to the formation of space charge in the vicinity of the grains [58]. Charged species, impurities and defects tend to segregate to the grain boundaries in order to minimize strain and lower electrostatic energies in the system.

4. Conclusion

Nanocrystalline PbSe thin films were deposited on glass substrates by electron beam evaporation technique. The XRD studies reveal that the films are polycrystalline in nature with cubic structure and preferential orientation along the (002) plane with lattice parameter a = 0.6134 (±0.001) nm. The crystallite sizes measured by XRD are found to be within nanometer scale. The optical transitions in all films have been found to be allowed and direct. The change in optical band gap with increase in the film thickness may be due to the decrease in the amount of disorder in the materials and decrease in the density of defects states.

Besides, the as-deposited thin films were found to be characterized as a semiconductor-like behavior.

References

[1] S.R. Gosavi, N.G. Dshpande, Y.G. Gudage, R. Sharma, J. Alloys Compd. 448 (2008) 344.
[2] A. Hmood, A. Kadhim, H. Abu Hassan, J. Alloys Compd. 520 (2012) 1.
[3] S.A. Khan, Z.H. Khan, A.A. El-Sebaii, F.M. Al-Marzouki, A.A. Al-Ghamdi, Physica B 405 (2010) 3384.
[4] S. Kumar, Z.H. Khan, M.A. Majeed, Khan M. Husain, Curr. Appl. Phys. 5 (2005) 561.

[5] B. Pejova, I. Grozdanov, A. Tanusevski, Mater. Chem. Phys. 83 (2004) 245.
[6] S. Kumar, B. Lal, P. Aghamkar, M. Husain, J. Alloys Compd. 488 (2009) 334.
[7] O.K. Tan, W. Cao, Y. Hu, W. Zhu, Solid State Ionics 172 (2004) 309.
[8] E.A. Albanesi, E.L. Peltzer y Blanca, A.G. Petukhov, Comput. Mater. Sci. 32 (2005) 85.
[9] Y. Sun, X. Qian, J. Yin, J. Huang, X. Ma, Z. Zhu, J. Mater. Res. 16 (2001) 2922.
[10] P.J. Taylor, N.K. Dhar, E. Harris, V. Swaminathan, Y. Chen, W.A. Jesser, J. Electron. Mater. 39 (2009) 2343.
[11] K.C. Sharma, R.P. Sharma, J.C. Garg, J. Phys. D. Appl. Phys. 25 (1992) 1019.
[12] T. Saitosh, S. Matsubara, S. Minagawa, Jpn. J. Appl. Phys. 16 (1977) 807.
[13] H. Zogg, M. Arnold, Infrared Phys. Technol. 49 (2007) 183.
[14] M.C. Torquemada, M.T. Rodrigo, G. Vergara, F.J. Sánchez, R. Almazán, M. Verdú, P. Rodríguez, V. Villamayor, L.J. Gómez, M.T. Montojo, A. Muñoz, J. Appl. Phys. 93 (2003) 1778.
[15] S.A. Saleh, A. Al-Hajry, H.M. Ali, Phys. Scr. 84 (2011) 015604.
[16] W. Ren, W. Cao, S. Wang, M. Sui, H. Lu, J. Alloys Compd. 509 (2011) 5947.
[17] J. Dheepa, R. Sathyamoorthy, S. Velumani, A. Subbarayan, K. Natarajan, P.J. Sebastian, Sol. Energy Mater. Sol. Cells 81 (2004) 305.
[18] A.Y. Ueta, G. Springholz, F. Schinagl, G. Marschner, G. Bauer, Thin Solid Films 306 (1997) 320.
[19] Roman T. Rumianowskia, Roman S. Dygdala, Wojciech Jung, Waclaw Bala, J. Cryst. Growth 252 (2003) 230.
[20] D.M. Ma, C. Cheng, J. Alloys Compd. 509 (2011) 6595.
[21] L. Weizhong, J. Alloys Compd. 493 (2010) 358.
[22] E. Steinbeiss, in: M.J. Thornton, M. Ziese (Eds.), Spin Electronic, Springer-Verlag, Berlin Heidelberg, Germany, 2001, p. 298.
[23] L.M. Goncalves, C. Couto, P. Alpuim, A.G. Rolo, F. Völklein, J.H. Correia, Thin Solid Films 518 (2010) 2816.
[24] D.A.P. Bulla, R.P. Wang, A. Prasad, A.V. Rode, S.J. Madden, B. Luther-Davies, Appl. Phys. A96 (2009) 615.
[25] D.K. Ivanov, N.P. Osipovich, S.K. Poznyak, E.A. Streltsov, Surf. Sci. 1092 (2003) 532.
[26] D.P. Pasiyan, A. Marikani, K.R. Murall, Cryst. Res. Technol. 35 (2000) 949.
[27] A.M. Salem, T.M. Dahy, Y.A. El-Gendy, Physica B 403 (2009) 3027.
[28] A.R. Balu, V.S. Nagarethinam, A. Thayumanavan, K.R. Murali, C. Sanjeeviraja, M. Jayachandran, J. Alloys Compd. 502 (2010) 434.
[29] A.A.M. Farag, I.S. Yahia, E.G. El-Metwally, J. Optoelectron. Adv. Mater. 11 (2009) 204.
[30] B.R. Sankapal, C.D. Lokhande, Mater. Chem. Phys. 74 (2002) 126.
[31] S.A. Saleh, A.A. Hendi, I.A. Abdel-Latif, J. Am. Sci. 7 (2011) 923.
[32] M. Saleem, L. Fang, A. Wakeel, M. Rashad, C.Y. Kong, World J. Condens. Matter Phys. 2 (2012) 10.
[33] S. Kumar, B. Lal, S. Rohilla, P. Aghamkar, M. Husain, J. Alloys Compd. 505 (2010) 334.
[34] L. Meng, H. Meng, W. Gog, W. Liu, Z. Zhang, Thin Solid Films 519 (2011) 7627.
[35] Y. Badr, I.K. Battisha, A.M.S. El Nahrawy, B. Elouadi, M. Kamal, N. J. Glas. Ceram. 1 (2011) 71.
[36] F. Gu, S.F. Wang, M.K. Lu, G.J. Zhou, D. Xu, D.R. Yuan, J. Phys. Chem. B 108 (2004) 8119.
[37] Z.R. Khan, M. Zulfequar, M.S. Khan, Mater. Sci. Eng. B 147 (2010) 145.
[38] N. El-Kadry, A. Ashour, S.A. Mahmoud, Thin Solid Films 269 (1995) 112.
[39] R. Tintu, V.P.N. Nampoori, R. Radhakrishnan, S. Thomas, Opt. Commun. 284 (2011) 222.
[40] F. Yakuphanoglu, S. Ilican, M. Caglar, Y. Caglar, Superlattice. Microst. 47 (2010) 732.
[41] N. Tingau, Cryst. Res. Technol. 43 (2008) 9964.
[42] C. Karunakaran, S.S. Raadha, P. Gomathisankar, J. Alloys Compd. 549 (2013) 269.
[43] H.M. Ali, M.M. Abou-Mesalam, M.M. El-Shorbagy, J. Phys. Chem. Solids 71 (2010) 51.
[44] J. Tauc, Amorphous and Liquid Semiconductors, Plenum Press, London and New York, 1974.
[45] G. Saffarini, J.M. Saiter, H. Schmitt, Opt. Mater. 29 (2007) 1143.
[46] V. Pamukchieva, A. Szekeres, K. Todorova, E. Svab, M. Fabian, Opt. Mater. 32 (2009) 45.
[47] M. Fadel, S.A. Fayek, M.O. Abou-Helal, M.M. Ibrahim, A.M. Shakra, J. Alloys Compd. 485 (2009) 604.
[48] S.A. Khan, F.A. Al-Agel, A.A. Al-Ghamdi, Superlattice. Microst. 47 (2010) 695.
[49] T.M. Hammad, J.K. Salem, R.G. Harrison, Superlattice. Microst. 47 (2010) 335.
[50] H.A. Mohamed, H.M. Ali, Sci. Technol. Adv. Mater. 9 (2008) 025016.
[51] S.H. Mohamed, H.M. Ali, J. Appl. Phys. 109 (2011) 1.
[52] H.M. Ali, Phys. Status Solidi A 202 (14) (2005) 2742.
[53] S.H. Wemple, M. DiDomenico, Phys. Rev. B3 (1971) 1338.
[54] M.M. Wakkad, E.Kh. Shoker, S.H. Mohamed, J. Non-Cryst. Solids 265 (2000) 157.
[55] J.M. Xu, S. Wang, H.L. Ding, S.S. Pan, Y.X. Zhang, G.H. Li, Mater. Res. Bull. 47 (2012) 4457.
[56] S.A. Ansari, A. Nisar, B. Fatma, W. Khan, M. Chaman, A. Azam, A.H. Naqvi, Mater. Res. Bull. 47 (2012) 4161.
[57] E. Prokhorov, A. Mendoza-Galván, J. González-Hernández, B. Chao, J. Non-Cryst. Solids 353 (2007) 1870.
[58] I. Lubomirsky, J. Fleig, J. Maier, J. Appl. Phys. 92 (2002) 6819.